Journal of Hazardous Materials 476 (2024) 134887

Contents lists available at ScienceDirect

Journal of Hazardous Materials

journal homepage: www.elsevier.com/locate/jhazmat

Optimization of polyethylene terephthalate biodegradation using a self-assembled multi-enzyme cascade strategy

Lizhu Aer [a], Qifa Jiang [a], Linling Zhong [a], Qiuyue Si [a], Xianghong Liu [a], Yan Pan [c], Juan Feng [a,b], Hongjuan Zeng [a,b], Lixia Tang [a,b,*]

[a] School of Life Science and Technology, University of Electronic Science and Technology of China, Chengdu 610054, China
[b] Center for Informational Biology, University of Electronic Science and Technology of China, Chengdu 610054, China
[c] Medical School of University of Electronic Science and Technology of China, Chengdu 610054, China

HIGHLIGHTS

- Multi-enzyme complexes (PT-ECs) exhibit efficient PET degradation at 40 ℃.
- The activity of PT-EC^{EHA} in degrading PET is 16.5-fold more than that of PETase^{EHA}.
- Surface-displayed PT-EC^{EHA} has 20-fold higher activity than displayed PETase^{EHA}.
- Surface-displayed PT-EC enhances enzyme tolerance against organic solvent.
- TfCa$^{I69W/L281Y}$ enhances the surface-displayed PT-EC enzyme activity by 2.5-fold.

GRAPHICAL ABSTRACT

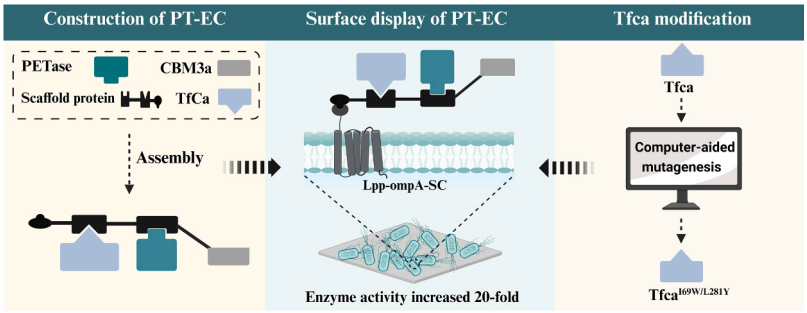

ARTICLE INFO

Keywords:
*Is*PETase
TfCa
PET degradation
Multi-enzyme cascade
Surface display

ABSTRACT

Although many efforts have been devoted to the modification of polyethylene terephthalate (PET) hydrolases for improving the efficiency of PET degradation, the catalytic performance of these enzymes at near-ambient temperatures remains a challenge. Herein, a multi-enzyme cascade system (PT-EC) was developed and validated by assembling three well-developed PETases, PETase^{EHA}, Fast-PETase, and Z1-PETase, respectively, together with carboxylesterase TfCa, and hydrophobic binding module CBM3a using scaffold proteins. The resulting PT-EC^{EHA}, PT-EC^{FPE}, PT-EC^{ZPE} all demonstrated outstanding PET degradation efficacy. Notably, PT-EC^{EHA} exhibited a 16.5-fold increase in product release compared to PETase^{EHA}, and PT-EC^{ZPE} yielded the highest amount of product. Subsequently, PT-ECs were displayed on the surface of *Escherichia coli*, respectively, and their degradation efficiency toward three PET types was investigated. The displayed PT-EC^{EHA} exhibited a 20-fold increase in degradation efficiency with PET film compared to the surface-displayed PETase^{EHA}. Remarkably, an almost linear increase in product release was observed for the displayed PT-EC^{ZPE} over a one-week degradation period, reaching 11.56 ± 0.64 mM after 7 days. TfCa$^{I69W/L281Y}$ evolved using a docking-based virtual screening strategy showed a further 2.5-fold increase in the product release of PET degradation. Collectively, these advantages of PT-EC demonstrated the potential of a multi-enzyme cascade system for PET bio-cycling.

* Correspondence to: School of Life Science and Technology, University of Electronic Science and Technology of China, No. 4, Section 2, North Jianshe Road, Chengdu, China.
E-mail address: lixiatang@uestc.edu.cn (L. Tang).

https://doi.org/10.1016/j.jhazmat.2024.134887
Received 4 February 2024; Received in revised form 4 June 2024; Accepted 10 June 2024
Available online 11 June 2024

1. Introduction

Polyethylene terephthalate (PET) plastic, an extensively utilized polymer [1], poses an escalating environmental challenge attributed to the increasing accumulation of PET waste, thereby jeopardizing ecological systems and human health [2,3]. Traditional physical and chemical PET recycling methods suffer from drawbacks such as secondary environmental pollutants, high energy consumption, and substantial economic expenses [4,5]. In contrast, bio-recycling provides a "green channel" for PET recycling due to its simplicity of operation, environmental and energy-saving characteristics [6].

Over the past decade, various PET hydrolyzing enzymes, including lipases, esterases, carboxylesterases, and cutinases, have been identified [1,7,8]. These enzymes convert PET into a mixture of bis(hydroxyethyl) terephthalate (BHET), mono-2-hydroxyethyl terephthalate (MHET), terephthalic acid (TPA), and ethylene glycol (EG). However, their PET degradation efficacy is often limited to the near glass transition temperature ($T_g = 75$ °C) [6]. A significant breakthrough occurred in 2016 when Yoshida et al. successfully isolated PET hydrolase, identified as *Is*PETase, from the bacterium *Ideonella sakaiensis* [9]. The paramount attribute of *Is*PETase resides in its PET degradation activity at ambient temperature. This distinctive characteristic renders *Is*PETase the most promising approach for achieving sustainable PET bio-recycling. However, the wild-type *Is*PETase still suffered from the limitations of poor thermal stability and activity. To address these issues, several pioneering studies have been conducted [10–12]. For instance, through structure-based design using machine learning algorithms, Dura-PETase and Fast-PETase exhibited significant melting temperature (T_m) increases of 31 °C and 21.1 °C, respectively [13,14], Dura-PETase completely biodegraded 2 g/L microplastics into water-soluble products at 37 °C and Fast-PETase effectively degraded the amorphous portion of commercial bottles and the entire heat-treated water bottles at moderate temperatures (50 °C). Through directed evolution, the obtained DepoPETase and HotPETase exhibited elevated T_m values of 23.3 °C and 34.4 °C, respectively, demonstrating excellent degradation efficiency for untreated and semi-crystallized post-consumer PET at moderate and near glass transition temperatures [15,16]. Additionally, PETase^{EHA} and Z1-PETase, derived from structural analysis of *Is*PETase, displayed increased T_m of 8.81 °C and 25 °C, respectively, and demonstrated excellent degradation capability at near ambient temperature (40 °C). Particularly, Z1-PETase showed high accessibility of among mesophilic PET hydrolase and fast depolymerization rate at higher temperatures [17,18]. Despite these advances, the catalytic properties of these enzymes at near ambient temperatures needs to be further improved.

In addition to mutagenesis analysis, to further improve the efficiency of PET degradation by *Is*PETase at near-ambient temperatures, the focus turns to addressing challenges arising from both product inhibition and substrate adsorption [19]. The utilization of multiple enzyme cascades stands as a promising strategy to mitigate these inhibitory effects, while gaining the advantage of promoting enzyme proximity effects, thereby enhancing PET degradation [20,21]. Recent studies have emphasized that facilitating MHET conversion can further improve PET degradation efficiency since MHET greatly inhibits the activity of *Is*PETase [22–24]. Although MHETase exhibits a high activity toward MHET, its poor soluble expression greatly impedes its application as a biocatalyst [25]. To overcome this challenge, TfCa, a carboxylesterase from *Thermobifida fusca*, was adopted to replace the function of MHETase [26]. The enzyme demonstrated high activity toward the intermediates produced during the hydrolysis of PET, such as BHET and MHET. When TfCa was combined with *Is*PETase, it resulted in a 4.2-fold increase in total product release and an 11-fold increase in TPA release from degraded PET film, indicating that TfCa could effectively mitigate the inhibitory effect of MHET on *Is*PETase [26].

Moreover, in heterogeneous hydrolysis reaction systems, enzymatic degradation usually involves a two-step process: enzyme binding to the substrate and subsequent hydrolytic cleavage [27]. The substrate binding step has been proven to be particularly important in determining the catalytic efficiency of the enzyme [28]. For instance, cellulosomes exhibit highly efficient degradation of cellulose due to the presence of a substrate-binding module CBM. This module has been shown its significance in breaking down several other hydrophobic solid substrates [29,30]. However, through the examination of the crystal structure of *Is*PETase, it becomes evident that *Is*PETase does not possess a conspicuous substrate-binding motif. Some hydrophobic binding modules fused to enzymes have been reported to improve enzyme efficiency by increasing the adsorption capacity of the enzyme onto the polymer [29,31]. Chen et al. constructed a yeast co-display system with both hydrophobic adhesion module HFBI and *Is*PETase degradation module for efficient degradation of highly crystalline PET (crystallinity 45 %) at 30 °C [32]. Additionally, when a relatively hydrophobic NusA tag fused with PETase^{EHA}, NusA-PETase^{EHA} showed a significant increase in the hydrophobic binding capacity to PET film, resulting in a 1.4-fold higher product release compared to PETase^{EHA} alone [33]. Overall, the above examples demonstrated that the combination of *Is*PETase with adsorption modules will greatly enhance PET degradation efficiency.

The efficient assembly of the above modules is another important issue. It is well known that some anaerobic bacteria achieve high cellulose degradation through a cellulosome multi-enzyme self-assembly system [30,34]. In the system, cellulases containing dockerin modules were assembled through the interaction with cohesin modules of scaffolding proteins [35]. This system has been adopted in several cases for efficient multi-enzyme cascade biocatalysis [36]. Thus, the use of scaffolding proteins to assemble PET hydrolases and hydrophobic binding modules into complexes might be a promising choice to address the above challenges.

In this study, a multiple enzyme complex, designated as PT-EC, was constructed by integrating CBM3a, derived from the hydrophobic binding module of *Clostridium thermocellum* [34], TfCa from *Thermobifida fusca*, and three types of PETases, respectively, utilizing cellulosome scaffolding proteins. All three constructed PT-ECs exhibited superior PET degradation ability, which was subsequently displayed on the surface of *Escherichia coli* (*E. coli*) using a cellulosome multi-enzyme self--assembly system. The resulting displayed PT-ECs showed not only the higher PET depolymerization efficacy at 40 °C, but also a higher tolerance against organic solvent, compared to the surface-displayed PETase^{EHA} alone. This investigation introduces a rational assembly of diverse functional units on microbial surface to improve biocatalytic efficiency, offering a valuable strategy for applications in biocatalysis, biosensing, and bioenergy.

2. Materials and methods

2.1. Materials

The PET film (amorphous, 0.25 mm thickness) employed in this study was sourced from Goodfellow GmbH (London, UK), and the PET powder originated from DuPont Co., Ltd (Shanghai, China). PET bottles were derived from Nestle, Pepsi-cola, and Nongfu Spring. Chemicals, namely bis(hydroxyethyl) terephthalate (BHET), hydroxyethyl terephthalate (MHET), and terephthalic acid (TPA), were procured from Aladdin Biochemical Technology Co., Ltd. (Shanghai, China). Isopropyl β-D-thiogalactopyranoside (IPTG), L-arabinose, methanol, trifluoroacetic acid dimethyl sulfoxide (DMSO) and other biochemical reagents were acquired from Aladdin Biochemical Technology Co., Ltd. Plasmid vectors, including pGro7 and pET30a, and bacterial strains such as *E. coli* BL21 (DE3), *E. coli* DH5α, and Shuffle T7 strains, are stored in the laboratory.

2.2. Protein expression and purification

Genes encoding PETases, TfCa, DocT-PETases, DocB-TfCa, DocB-MHETase and the scaffolding protein cohesion-TB (with or without CBM3a) were cloned into the pET30a expression vector to generate corresponding expression vectors. The resulting expression vectors were co-transfected with plasmid pGro7, carrying the GroEL/ES molecular chaperone gene, into *E. coli* shuffle T7 cells. Co-transformants were cultured on LB agar plates supplemented with chloramphenicol and kanamycin overnight. Monoclonals were picked into 20 mL of LB medium for 12 h, followed by transfer to 2 % (v/v) TB medium and incubation for 3 h at 37 °C with agitation at 220 rpm. When reaching the bacterial optical density OD_{600} of 1.5, the temperature was lowered to 16 °C, and induction of recombinant proteins and molecular chaperone proteins was initiated by adding 0.5 mM IPTG and 1 g/L L-arabinose, respectively, for a 24-h induction period.

After induction, cells were harvested by centrifugation at 4000g for 15 min, and the resulting pellet was resuspended in buffer A (50 mM Tris-HCl, 150 mM NaCl, pH 7.5). Ultrasonication (200 W, break for 1 s, stop for 1 s) was employed for cell disruption. Subsequent centrifugation at 4 °C and 13500g for 45 min removed cell debris. The resulting supernatant, filtered through a 0.22 μm membrane, underwent purification via affinity chromatography using a HisTrap column. Protein loading was conducted with buffer A containing 10 mM imidazole, followed by washing with buffer A containing 30 mM imidazole to eliminate non-specifically bound proteins. Elution of the target proteins was achieved using buffer A containing 300 mM imidazole. For the assembly of the PT-EC complex, the proteins were concentrated and quantified using the Bradford assay. Next, they were combined in a binding buffer consisting of 50 mM glycine-NaOH (pH 9.0) and 15 mM $CaCl_2$, followed by incubation for 3 h at 25 °C [34].

2.3. Surface display of the multi-enzyme complex on E. coli

The construction of the surface display expression vector involved fusing the Spy-catcher (SC) gene to the C-terminus of the Lpp-ompA gene, which was then cloned into pET30a. Its expression conditions were outlined in Section 2.2, with the exception that the expression of molecular chaperone was not involved, and induction was carried out at 25 °C for 20 h. For functional assessment, bacteria expressing Lpp-ompA-SC underwent triple washing with buffer A. An excess of Spy-tag (ST) fused green fluorescent protein (ST-GFP) was then added. The mixture was incubated with oscillation at 25 °C and 350 rpm for 3 h (the volume of the mixture was 0.8 mL, and the $OD_{600} = 1$). Following incubation, centrifugation and triple washing were performed, and the quantity of ST-GFP loaded onto the surface display system was determined. The functionality of the surface display system was evaluated using a fluorescence spectrophotometer and fluorescence microscope. The fluorescence spectrophotometer employed an excitation wavelength of 485 nm, with excitation light scanning from 500 - 800 nm, a slit of 5 nm, and a voltage of 700 V.

To construct a PT-EC self-assembled whole-cell biocatalytic system, *E. coli* expressing Lpp-ompA-SC were supplemented with different concentrations of scaffolding proteins (cohesion-TB) fused with Spy-tag and shaken at 25 °C for 3 h. Unassembled scaffold proteins were subsequently washed away. DocT-PETase and DocB-TfCa were then added in equimolar proportions to a whole-cell assembly system containing 15 mM $CaCl_2$ and self-assembly was allowed for 3 h at 25 °C. The whole-cell assembly system was washed three times with Buffer A to remove unassembled proteins.

2.4. Crystalinity measurement of PET samples

The crystallinity of the PET sample was analyzed using a differential scanning calorimetry instrument (DSC250, TA Instrument). Initially, 5 mg of PET samples were prepared and equilibrated at 30 °C for 2 min. Subsequently, the PET samples were heated from 30 °C to 300 °C at a rate of 10 °C/min [18]. The enthalpies of melting and cold crystallization were employed to determine the degree of crystallinity of the PET using the following equation:

$$X_c\ (\%) = [(\Delta H_m - \Delta H_c) / \Delta H_m \times 100\%] \times 100\%$$

where ΔH_m is the enthalpy of melting (J/g), ΔH_c is the enthalpy of cold crystallization (J/g), and $\Delta H_m \times 100$ % is the enthalpy of melting of a 100 % crystalline PET, which is 140.1 J/g.

2.5. Preparation of bottle-derived PET powder

Bottle-derived PET powder (crystallinity 12.5 %) was prepared from commercial post-consumer water bottles (Pepsi-cola, Nongfu Spring, Chengdu, China). The detailed steps were as follows: the bottles were melted in a muffle furnace at 280 °C for 10 min and rapidly cooled in ice water. The resulting PET samples were then immersed in liquid nitrogen for 5 min and then ground into pellets, which were subsequently sieved through a 50-mesh sieve to obtain powders with a diameter of 280 μm or less.

2.6. Enzyme assays for PET

To assess the functionality of PT-EC, enzyme activity was conducted using various PET substrates, including amorphous PET film (crystallinity 5.67 %), commercial PET powder (crystallinity 48.1 %), bottle-derived PET powder (crystallinity 12.5 %) and diverse commercial PET bottles (crystallinity 30 – 40 %). PET films were precision-punched into 0.8 mm diameter discs using a perforator and then washed with 70 % ethanol for 30 min. Each PET film possessed a thickness of 0.25 mm and an average weight of 15 mg. A piece of PET film or 15 mg PET powder was then placed into 0.8 mL of Gly-NaOH buffer (pH 9) containing 100 nM enzyme and reacted for varying periods at 40 °C. For the validation of PET degradation by whole-cell biocatalytic system, PET was directly added to 0.8 mL of an *E. coli* whole-cell biocatalytic system ($OD_{600} = 1$) displaying enzymes on the surface. To explore the impact of pH on enzyme activity, different buffer systems were employed: 100 mM $C_6H_8O_7$-$C_6H_9Na_3O_9$ buffer (pH 3.0 – 6.0), 100 mM Na_2HPO_4-NaH_2PO_4 buffer (pH 6.0 – 8.0), 100 mM Tris-HCl buffer (pH 8.0 – 9.0), 100 mM Gly-NaOH (pH 9 – 11) and 100 mM Na_2HPO_4-NaOH (pH 11 – 12).

Upon completion of the depolymerization reaction, PET films underwent sequential washing with 1 % SDS for 30 min, 70 % ethanol for 30 min, and deionized water for 30 min. The washed PET films were subsequently desiccated at 40 °C overnight. Morphological changes in the PET films were observed using a scanning electron microscope (Zeiss Gemini SEM 300, Germany) with an electron beam intensity of 3.0 kV.

For the gram-scale PET degradation test, the bottle-derived PET powder (crystallinity 12.5 %) was placed in a customized laboratory-scale bioreactor. Temperature regulation was achieved using a heating circulator (BC-206E, Labtop, China), while pH monitoring utilized a digital display pH electrode (PHG-21 C, Lei-ci, China) with 0.01 increments and calibrated at pH 6.86 and pH 9.21. For the reaction, 0.5 μM PT-EC or Z1-PETase was added to 100 mL of 100 mM Gly-NaOH (pH 9) with a concentration of 2.5 % (w/v) of the bottle-derived PET powder, and the reaction was triggered at 40 °C. The pH of the reaction was maintained between 8.5 and 9.0 by adding 2 M NaOH. Samples were periodically taken for HPLC analysis. After completion, the reaction solution was filtered using a 0.45 μm filter membrane. The residual bottle-derived PET powder was then dried at 50 °C, and the weight loss was subsequently calculated.

2.7. Enzyme assays for MHET

To characterize the TfCa and its mutants, enzyme activity was

assessed in a 0.6 mL phosphate buffer (pH 7.5) reaction system containing 5 mM MHET as model substrates. The degradation reaction commenced with the addition of 500 nM purified enzyme to the reaction, followed by incubation at 40 °C for 12 h. Following the completion of each reaction, termination was achieved by adding 300 μL of methanol to the reaction mixture. The termination reactions were subsequently validated using high-performance liquid chromatography (HPLC).

2.8. HPLC analysis of the degradation products

Following the completion of the reaction, HPLC analysis was performed with minor adaptations to previously established protocols [21]. The reaction mixture was centrifuged at 13,000g for 10 min, and the resultant supernatant underwent detection using an HPLC system featuring integrated separation and detection (SHIMADZU LC-2050). Separation occurred on a ShimNex CS C18 column (5 μm, 4.6 × 250 mm) at 25 °C. Mobile phases consisted of buffer A (0.1 % aqueous trifluoroacetic acid) and buffer B (methanol) at a flow rate of 0.8 mL/min. The elution conditions encompassed a linear gradient of methanol, transitioning from 5 % to 40 % over 0 to 5 min, followed by an elevation from 40 % to 45 % between 5 to 18 min, and ultimately a reduction from 45 % to the initial 5 % within 18 – 22 min. Analytes, including BHET, MHET, and TPA, were detected at 260 nm.

2.9. Molecular docking-based virtual screening

Sixty-six amino acids situated within a 10 Å radius of the active center of TfCa (PDB-ID: 7W1K) were selected as mutation sites. Virtual saturated amino acid mutagenesis was conducted using the Build Model command in the FoldX software [37]. Molecular docking of MHET to receptor proteins (TfCa and its mutants) was performed using AutoDock Vina 1.2.0 software [38]. Before molecular docking, MHET was hydrogenated and its torsion bonds were thoroughly examined. The receptor proteins underwent a sequential process involving the removal of water molecules, the addition of hydrogen atoms, Gasteiger charge calculations, and assignment of AD4 atom types. All molecular docking simulations were executed within a box with a side length of 50 Å centered around the active site. Following the completion of molecular docking, mutants exhibiting low docking free energy were selected for validation of MHET degradation.

2.10. Molecular dynamics simulations

The complexes $TfCa^{WT}$-MHET and $TfCa^{I69W/L281Y}$-MHET were subjected to simulations in Gromacs2022.3 utilizing the amber99sb-ildn force field [39,40]. AmberTools22 was used to add a generation amber force field (GAFF) to the MHET. Gaussian 16 W was utilized for MHET hydrogenation and restrained electrostatic potential (RESP) calculation. The simulation conditions were maintained at a static temperature of 300 K and atmospheric pressure (1 Bar). Solvation was achieved using water molecules (Tip3p water model), and the overall charge of the simulation system was neutralized by adding an appropriate number of Na^+ ions. Following equilibration under the isothermal isovolumetric ensemble (NVT) and isothermal isobaric ensemble (NPT), free molecular dynamics simulations were conducted. The simulation involved 5000,000 steps, with a step length of 2 fs, spanning a total duration of 100 ns. Subsequently, the software's built-in tools were used to analyze data such as root-mean-square deviation (RMSD), root-mean-square fluctuation (RMSF) and combined with free energy (MMGBSA).

3. Results and discussion

3.1. Self-assembly of a multi-enzyme cascade system

*Is*PETase possesses a more expansive hydrophobic activity pocket, facilitating the degradation of PET at ambient temperatures [41,42]. However, the efficacy of *Is*PETase and its mutants in degrading PET at ambient temperatures needs to be further improved. To address its limitations, a multi-enzyme complex system, denoted as PT-EC, was ingeniously structured (Fig. 1A and B). This system was composed of PETase, TfCa, and CBM3a assembled via cellulosome scaffolding proteins for the hydrolysis of PET and the degradation of intermediate MHET. To evaluate the feasibility of the system, three well evolved *Is*PETase mutants $PETase^{EHA}$, Fast-PETase, and Z1-PETase were adopted. The corresponding PT-ECs were termed as $PT\text{-}EC^{EHA}$, $PT\text{-}EC^{FPE}$, and $PT\text{-}EC^{ZPE}$, respectively. For the construction, a hybrid basic scaffold protein (cohesin-TB) was engineered by fusing cohesion-T from *Clostridium thermocellum* with cohesion-B from *Bacteroides cellulosolvens*, and CBM3a was fused to the N-terminus of the cohesion-T. Meanwhile, the dockerin modules of different origins were fused to PETases and TfCa, respectively, with a flexible linker (GGGGS) used to prevent mutual interference between dockerin and target proteins (Fig. S1 and Table. S1). The functional assessment of PT-ECs showed their remarkable PET degradation efficiency. After 48 h of degradation with 100 nM of enzyme at 40 °C. $PT\text{-}EC^{EHA}$ released 2.79 ± 0.36 mM of product, exhibiting a 16.5-fold increase compared to $PETase^{EHA}$ alone. Similarly, the product released from $PT\text{-}EC^{FPE}$ was 3.16 ± 0.15 mM, which was 6.6-fold of that of Fast-PETase alone. Moreover, $PT\text{-}EC^{ZPE}$ released 4.3 ± 0.1 mM of product, the highest amount of released product among the three tested PT-ECs, indicating a 3.4-fold increase compared to Z1-PETase alone (Fig. 1C).

To gain a comprehensive insight into the multi-enzyme complex, the function of each module was verified. Employing an equimolar mixture of $PETase^{EHA}$ and TfCa for PET degradation resulted in a 4-fold increase in product release compared to $PETase^{EHA}$ alone. Also, the incorporation of TfCa increased the product release of Fast-PETase and Z1-PETase by 2.8-fold and 1.3-fold, respectively, relative to the enzymes alone (Fig. 1C). Notably, it was noticed that the product release in the above three reactions contained a larger fraction of TPA compared to that catalyzed by PETase alone, which correlated well with the function of TfCa that converts MHET to TPA [26]. Furthermore, the activity of TfCa for MHET conversion was compared with MHETase. The results showed that both enzymes produced similar amounts of TPA after reaction at 40 °C for 12 h (Fig. S2), suggesting that the activity of the two enzymes toward MHET is comparable under the above tested conditions. Therefore, TfCa could be used as an alternative to MHETase in PET degradation to facilitate the conversion of MHET to TPA, which in turn might mitigate the inhibitory effect of MHET [26].

To validate the role of scaffolding proteins and CBM3a in the multi-enzyme cascade system, the corresponding CBM3a-free multi-enzyme complexes ($PT\text{-}ECs^{\Delta CBM}$) of three PETases were constructed. The PET degradation capacity of the resulting complexes retained only 56 % to 67 % activity of that of PT-ECs (Fig. 1C). The results suggested that the presence of the CBM3a module might modulate the function of PETases in PET degradation. The effects of CBM domain on the function of cellulase, PETase, and Leaf-branch compost cutinase (LCC) were also observed, which might be attributed by promoting substrate binding [43–46]. Moreover, $PT\text{-}ECs^{\Delta CBM}$ showed a 1.5- to 2.7-fold increase in product release compared to the equimolar mixture of PETase and TfCa (Fig. 1C), suggesting that a proximity effect of the dual enzymes that generate a substrate-catalyzed channel might be another reason to facilitate the reaction efficiency of multi-enzyme cascade reaction of PT-EC. Taken together, PT-EC system holds a promising potential in PET biodegradation over the free enzyme.

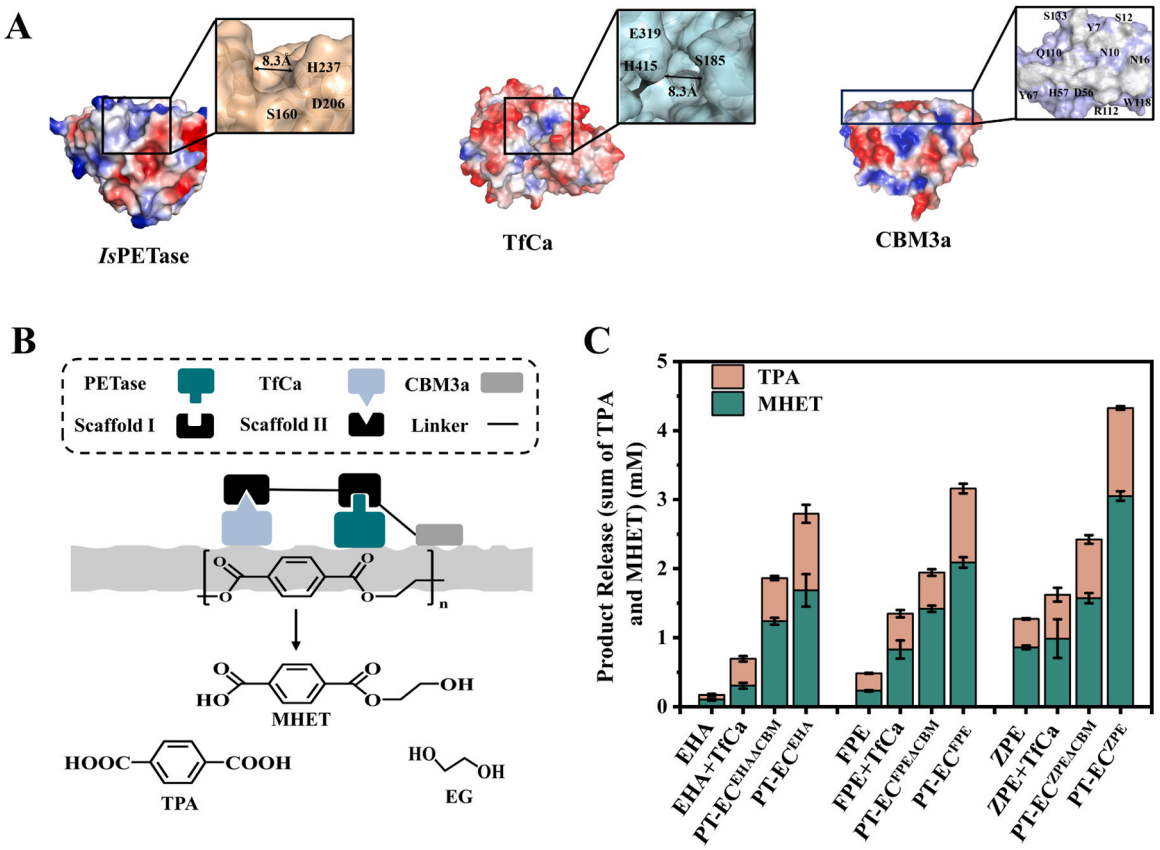

Fig. 1. The construction and functional verification of the multi-enzyme complex. (A) X-ray crystal structures of *Is*PETase (PDB-ID: 5XG0), TfCa (PDB-ID: 7W1J) (active pockets indicated by boxes), and CBM3a (PDB-ID: 4JO5) (hydrophobic binding region indicated by box). (B) Schematic diagram of the multi-enzyme complex system. (C) Assessment of product release by diverse enzymes during the degradation of bottle-derived PET powder (crystallinity 12.5 %) at 40 °C for 48 h. EHA represents PETase^{EHA}, FPE represents Fast-PETase, and ZPE represents Z1-PETase. $n = 3$ independent experiments. Data were presented as mean values ± SD.

3.2. Characterization of the multi-enzyme complex

The enzymatic properties of the constructed PT-ECs were investigated by using PT-EC^{EHA} as an example. For this, PET film (crystallinity 5.67 %) and bottle-derived PET powder (crystallinity 12.5 %) were used as model substrates (Fig. 2 and Fig. S3). Due to the fact that PETase catalyzed PET degradation in a concentration-dependent pattern, the optimal enzyme concentration for degradation of the above two substrates by PT-EC^{EHA} was determined (Fig. S4). For the degradation of a PET film with a diameter of 0.8 mm, the enzyme activity of PT-EC^{EHA} increased with rising enzyme concentration, reached a peak at 100 nM concentration, and then decreased with the further increase of enzyme concentration. In the case of 15 mg of PET powder, the enzyme activity gradually increased with the increase of enzyme concentration, and reached the maximum value when the enzyme concentration was 0.8 μM. Therefore, the following enzyme characterization experiments were carried out using the optimal enzyme concentration obtained above.

The results of temperature-dependent enzyme activity revealed an enhanced enzymatic activity for PT-EC^{EHA} over PETase^{EHA} across all temperatures tested, with 40 °C identified as its optimum reaction temperature, showing a similar pattern as PETase^{EHA} (Fig. 2A). The result indicated that PT-EC^{EHA} has a great potential to degrade PET at ambient temperature. Further analysis revealed that over the tested pH range of 5.0 to 12.0, PT-EC^{EHA} exhibited a dramatic increase in enzyme activity at pH 6, reaching its peak in the pH range of 8.5 – 10.0, followed by a sharp decline at pH > 10.5 (Fig. 2B). Although the optimal pH pattern of PT-EC^{EHA} was similar as that of PETase^{EHA}, PT-EC^{EHA} degraded PET with more efficiency at every pH tested compared to PETase^{EHA}.

The thermal stability of PT-EC^{EHA} was also evaluated. The results showed that the thermal stability of PT-EC^{EHA} was higher than that of PETase^{EHA}. PT-EC^{EHA} retained 64.9 % of residual activity after incubation at 40 °C for 24 h, and still retained 46.6 % of residual activity after 72 h, at which time the released product was 22.7-fold of that of PETase^{EHA}. However, PETase^{EHA} retained only 27.7 % residual activity after 24 h and only 8.9 % after 72 h (Fig. 2C). Moreover, a comparative analysis of the thermal stability of PT-EC^{EHA}, PT-EC^{EHAΔCBM}, and PETase^{EHA} revealed that both the scaffold protein assembly and the presence of CBM3a might be contribute to the enhancement of thermal stability of the multi-enzyme complex (Fig. S5A). Previous studies have also reported that the fusion of CBM family modules can enhance enzyme stability [47,48]. For instance, Zeng et al. fused CBM68 to the acid pullulanase PulB and showed a 3.5-fold increase in residual activity after incubation at 60 °C for 12 h compared to the unfused enzyme [49].

The tolerance results of the enzyme against organic solvents showed that PT-EC^{EHA} exhibited relatively low tolerance to all tested organic solvents compared to the control group, except for DMSO, which showed almost no negative effect on enzyme activity. Moreover, PT-EC^{EHA} exhibited higher activity than PETase^{EHA} in the presence of organic solvents except for Triton X-100 (Fig. 2D and Fig. S5B). In the presence of 5 % methanol and ethanol, the product release from PT-EC^{EHA} was 17- and 12.4-fold higher than that from PETase^{EHA}, respectively. In the case of 5 % DMSO, PT-EC^{EHA} demonstrated a 5.3-fold higher in product release than that of PETase^{EHA}. In the presence of 0.1 % Triton X-100, the enzyme activity of PT-EC^{EHA} was low, possibly due to the interaction of the hydrophobic unit of Triton X-100 with the multi-enzyme complex, which might interfere with the binding of the substrate to the active site. Taken together, PT-EC^{EHA} exhibited higher thermal stability and tolerance to organic solvents compared to

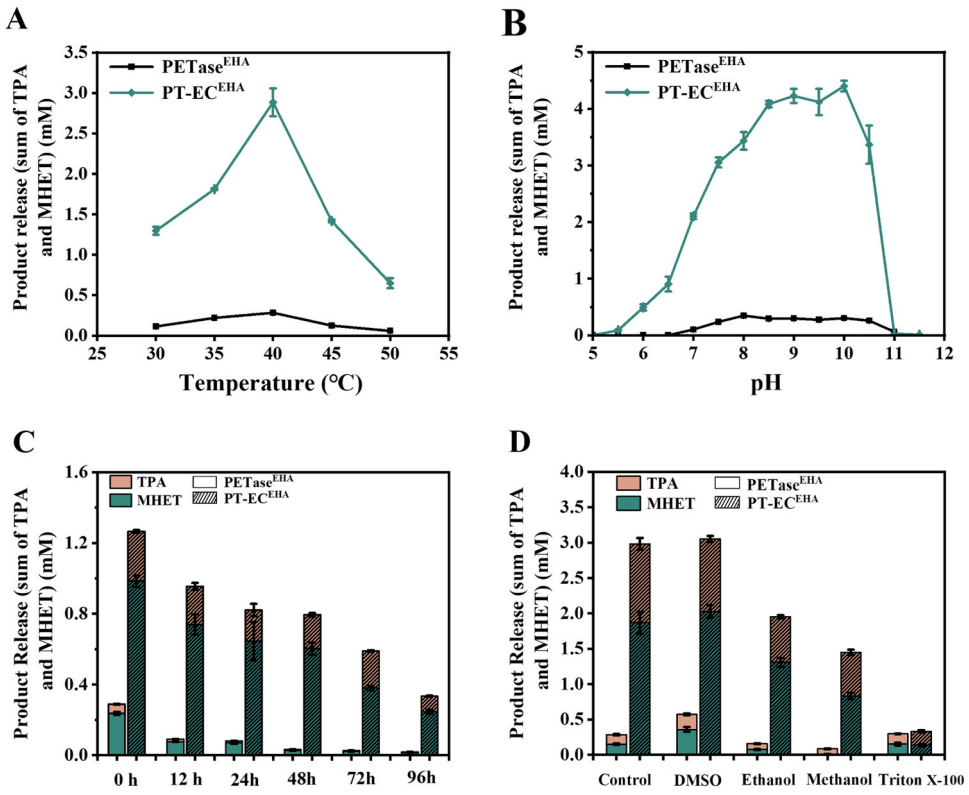

Fig. 2. Assessment of optimal temperature (A), optimal pH (B), thermal stability (C), and the tolerance against organic solvent (D) of PT-EC^{EHA} using bottle-derived PET powder (crystallinity 12.5 %) as the substrate. The reaction was carried out by adding 100 nM enzyme to 50 mM Gly-NaOH buffer (pH 9) at 40 °C for 48 h, except for the optimal pH analysis (buffer concentration of 100 mM) and the thermal stability analysis (40 °C, 10 h). $n = 3$ independent experiments. Data were presented as mean values ± SD.

PETase^{EHA} alone. Similar results were also observed in co-display of *Is*PETase with the hydrophobin HFBI, which showed an improvement of both the tolerance against organic solvents and thermal stability [32]. The above advantages of the multi-enzyme complex might be due to the introduction of scaffolding protein and hydrophobic protein, especially hydrophobic proteins, which have been proven to be able to maintain their functional activity in extreme environments [50].

3.3. Biodegradation of PET by the multi-enzyme complex

To further investigate the performance of PT-ECs in PET degradation, the degradation capacity of the constructed PT-ECs was monitored at 40 °C for 48 h with three types of PET. The results showed that the product release of all PT-ECs was 1.3- to 16.5-fold higher than that of the PETase alone toward all three types of PET (Fig. 3 and Fig. S6). With substrates bottle-derived PET powder (crystallinity 12.5 %) and commercial PET powder (crystallinity 48.1 %), PT-ECs displayed a similar degradation time-curve with PT-EC^{ZPE} showing the highest activity followed by PT-EC^{FPE} and PT-EC^{EHA} (Fig. 3A and B). In contrast, with PET film (crystallinity 5.67 %) as a substrate, PT-EC^{ZPE} showed the lowest activity among the three PT-ECs (Fig. 3C). Taken together, PT-EC^{ZPE} exhibited the highest degradation efficiency toward PET powder with low crystallinity, and about 1/3 lower efficiency for PET films with even lower crystallinity, while PT-EC^{FPE} and PT-EC^{EHA} both facilitated PET degradation with low crystallinity regardless of PET forms. The high degradation efficiency of PT-EC^{ZPE} might be due to the fact that the localized surface negative charge of the Z1-PETase, located far from the active site, repels the carboxylic acids in the PET powder, consequently increasing correct access orientation [18]. Furthermore, the high degradation efficiency of was PT-ECs also proved by scanning electron microscopy (SEM) analysis. The results showed that the PET films treated with PT-ECs exhibited a notably rough surface with morphological changes characterized by prominent erosion spots adorned with circular pits approximately 2.5 μm in size. In contrast, PET films treated solely with PETases displayed smaller erosion spots (Fig. S7). In conclusion, the advantages of PT-EC endowed its ability to degrade multiple forms of PET with high efficiency.

To further investigate the performance of PT-ECs in the long-term degradation of PET, the degradation of PET was monitored daily at 40 °C (Fig. S8). The results showed that the product release slowed sharply for all PT-ECs especially for PT-EC^{ZPE} after 2 days when degrading with substrates of bottle-derived PET powder and PET film. It is clear that the inactivation of Fast-PETase (T_m = 67.1 °C) and Z1-PETase (T_m = 74 °C) occurred after incubation at 40 °C for two days is unlikely. As is well known, for a long-term PET degradation system, in addition to enzyme product inhibition, acidification of the reaction will significantly decrease the activity of *Is*PETase [15,16]. Therefore, a bioreactor was customized to monitor the pH of the enzymatic reaction in real time (Fig. S9). For this, 100 mL reaction system containing 2.5 % (w/v) bottle-derived PET powder was used and the reaction was carried out at 40 °C with a pH range of 8.5 – 9.0. The product release of PT-EC^{ZPE} increased continuously throughout the measurement period for the first 8 days, whereas the product release of Z1-PETase increased continuously for the first 5 days and then reached equilibrium, which might be attributed to the higher thermal stability of PT-EC^{ZPE}. Their product releases after 10 days of degradation were 61.63 ± 0.19 mM and 41.84 ± 1.6 mM, respectively, corresponding to weight losses of 1.47 ± 0.02 g and 1.05 ± 0.04 g of PET powder, respectively (Fig. 3D). Thus, the results clearly indicated that the acidification of the reaction system greatly inhibited the enzyme activity for PET degradation. On the other hand, the results also implied that PT-EC system functioned well for PET degradation in a large scale.

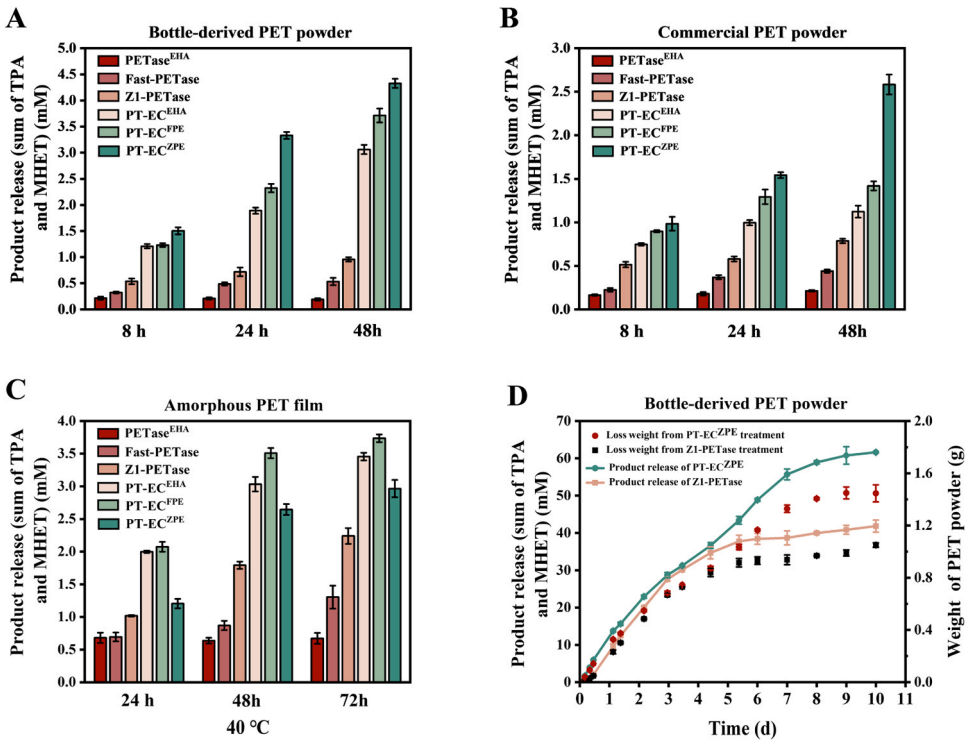

Fig. 3. Evaluation the degradation capabilities of PT-ECs to different PET types at 40 °C. (A), (B) and (C) represent the amounts of product release during the degradation of bottle-derived PET powder (crystallinity 12.5 %), commercial PET powder (crystallinity 48.1 %) and PET film (crystallinity 5.67 %), respectively. The reaction was conducted by adding either a piece of PET film or 15 mg of PET powder into 0.8 mL of 50 mM Gly-NaOH buffer (pH 9), supplemented with 100 nM enzyme, and maintained at 40 °C for different periods. (D) Evaluation of bottle-derived PET powder degradation in the bioreactor. The reaction was initiated by adding 0.5 μM of PT-EC^{ZPE} or Z1-PETase to 100 mL of 100 mM Gly-NaOH buffer (pH 9) containing 2.5 g of bottle-derived PET powder, followed by incubation at 40 °C. $n = 3$ independent experiments. Data were presented as mean values ± SD.

3.4. Surface display of the multi-enzyme complex on E. coli

The whole-cell biocatalytic system is widely favored for biocatalytic applications due to its reusability and resilience to certain extreme conditions [51,52]. For this purpose, a whole-cell biocatalytic system of PT-EC was developed by employing a surface display system involving both Lpp-ompA hybridization and bio-covalent ligation (Fig. 4A). Lpp-ompA is composed of a truncated *E. coli* lipoprotein Lpp (residues 1 – 9) fused to the first five β-strands of the outer membrane protein ompA (residues 46 – 159) [53]. Bio-covalent ligation Spy-catcher/Spy-tag system is covalently linked to the Spy-tag (ST) peptide through Asp-Lys [54]. For self-assembly of PT-EC on the surface of *E. coli*, Spy-catcher (SC) protein was fused to the C-terminus of Lpp-ompA, while ST was fused to the C-terminus of the scaffolding protein carrying PT-EC, with a flexible linker (GGGGS) maintaining the independence of each unit (Table S1).

Before surface display of PT-EC, the function of the self-assembled system was confirmed by displaying green fluorescent protein (GFP) for easy evaluation, with ST fused to the N-terminus of GFP. Following the incubation of the *E. coli* strain expressing Lpp-ompA-SC with purified ST-GFP, the cells show a distinct fluorescence emission peak at 510 nm with an excitation wavelength of 485 nm. Fluorescence microscopy analysis further confirmed that ST-GFP had been successfully ligated to the surface of *E. coli* (Fig. 4B). The amount of ST-GFP captured by SC was subsequently determined, the results demonstrated that surface-displayed SC exhibits outstanding protein capture capability, with 0.2 ± 0.05 mg of ST-GFP captured by the system (0.8 mL, $OD_{600} = 1$). Moreover, the above displaying efficiency could be easily manipulated by adjusting the amount of GFP added to the displayed reaction system. Thus, the surface-displayed Lpp-ompA-SC system offers a protein capture tool for displaying PT-EC with optimal enzyme concentration for effective PET hydrolysis since PET degradation efficiency by PETase displayed an enzyme-dependent pattern. The enzyme activity increases over a certain range of enzyme concentrations and decreases abruptly as the enzyme concentration increases, which may be due to spatial site barriers created by binding too much enzyme on the limited surface of PET [55].

PT-EC^{EHA} whole-cell biocatalytic system was subsequently constructed and optimized. For the surface-displayed PT-EC^{EHA} (0.8 mL, $OD_{600} = 1$), enzyme activity peaked at 1.28 μM PT-EC^{EHA} with PET film and at 1.5 μM PT-EC^{EHA} with PET powder as substrate (Fig. S10). Further analysis showed that the optimal temperature and pH of the surface-displayed PT-EC^{EHA} were the same as that of PT-EC^{EHA} (Fig. S11). The organic solvent tolerance of the surface-displayed PT-EC^{EHA} and none-displayed PT-EC were also evaluated using PET film as substrate (Fig. 4C). It was found that the surface-displayed PT-EC^{EHA} exhibited 95.2 % and 86.6 % of original activity in the reaction system containing 5 % ethanol and methanol, respectively, while none-displayed PT-EC^{EHA} retained approximately only 40 % of original activity in the two cases, indicating that the surface-displayed PT-EC^{EHA} exhibited better organic solvent tolerance ability than PT-EC^{EHA}, showing a promising potential for PET biodegradation.

The performance of displayed PT-ECs in the long-term degradation of PET was carried out at 40 °C. Using PET film (crystallinity 5.67 %) as a substrate, the product release of displayed PT-EC^{EHA} was linearly increased in the first 5 days, reaching 4.3 ± 0.02 mM after one week, which was 20-fold more than that of the surface display of PETase^{EHA} alone (Fig. 4D). The product release trend of the displayed PT-EC^{FPE} was similar to that of the displayed PT-EC^{EHA}. However, the activity of the displayed PT-EC^{ZPE} against PET film was very low (Fig. 4D). Considering the fact reported by Lee et al. that free Z1-PETase effectively degraded film at both 40 °C and 50 °C [18], our results might suggest that the morphology of the PET or the accessibility of the substrate is critical for the effective degradation of PET film by displayed PT-EC^{ZPE}. When using

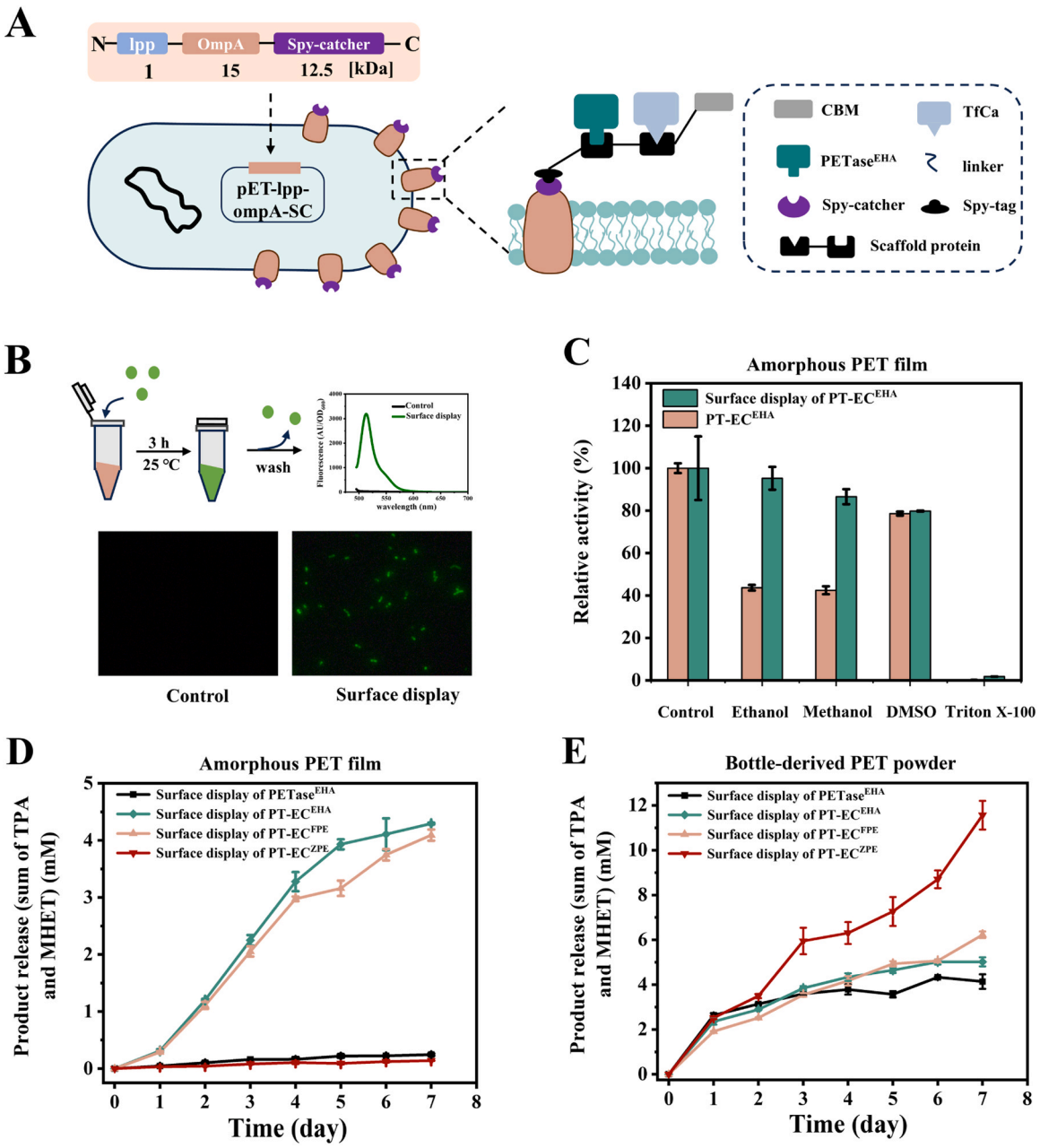

Fig. 4. Construction and functional verification of the surface-displayed PT-EC system. (A) Schematic diagram of the surface-displayed PT-EC system. (B) The functionality of surface-displayed SC was verified by fluorescence spectrophotometry and microscopy, Excess ST-GFP incubated with *E. coli* expressing Lpp-ompA-SC for 3 h at 25 °C. (C) Comparison of organic solvent tolerance of surface-displayed and none-displayed PT-EC^{EHA} in a reaction system containing 5 % organic solvent. In the absence of organic solvent, the relative activity of both was defined as 100 % and the product release was 1.3 ± 0.2 mM and 0.5 ± 0.01 mM, respectively. The reaction was incubated at 40 °C for 48 h using PET film as substrate. (D) and (E) represent the product release from the degradation of PET film and bottle-derived PET powder at 40 °C for one week, respectively. $n = 3$ independent experiments. Data were presented as mean values ± SD.

bottle-derived PET powder as substrate, the surface-displayed PT-EC^{ZPE} demonstrated notably higher enzyme activity compared to the other enzymes. Remarkably, a linear trend in product release was observed over a one-week degradation period, reaching 11.56 ± 0.64 mM after 7 days. The other three displayed PT-ECs demonstrated considerable degradation efficiency, with product release ranges between 4.1 mM and 6.0 mM (Fig. 4E). Thus, the results indicated that the morphology of PET substrate greatly determines the activity of both displayed and non-displayed PT-EC^{ZPE}, while the crystallinity is the main determinant for the activity of PT-EC^{FPE} and PT-EC^{EHA} in both displayed and non-displayed formats.

Moreover, for commercial PET bottles, the surface-displayed PT-EC^{EHA} facilitated the degradation of Nestle (crystallinity 30.1 %) and Pepsi-cola (crystallinity 39.5 %) commercial PET bottles with a 5.1- and 4.9-fold increase in degradation product release, respectively, compared to surface-displayed PETase^{EHA} alone (Fig. S12). Such an activity gap between displayed PT-EC^{EHA} and displayed PETase^{EHA} (around 5-fold) is smaller than that with amorphous PET films (20-fold), which might probably due to the crystallinity difference. Surprisingly, the surface-displayed PT-EC^{EHA} did not exhibit a similar promotional effect on the degradation of Nongfu Spring (crystallinity 35.9 %) plastic bottles. Considering the fact that all three types of bottles possess similar crystallinity, but probably different types of additives on their biodegradation ability might be the reasonable explanation [56]. In conclusion, the

surface-displayed PT-EC not only exhibited exceptional degradation prowess across diverse PET substrates, but also laid the foundation for upscaling conversion of degradation products using a "one-pot" strategy.

3.5. Structure-based enzyme engineering of TfCa

Although the cascade reaction of TfCa and PETase^{EHA} greatly improved the PET degradation efficiency, MHET was still present in the release product with a relatively high fraction. Thus, to enhance MHET degradation of TfCa, 66 amino acids within a 10 Å radius of the active center were subjected to single-point saturation mutagenesis. Molecular docking with MHET was performed for all mutants, and from 1320 (66 × 20) docking results, 9 mutants that ranked in the top 9 with low binding free energy were selected for further validation of MHET degradation. Among these mutants, the TfCa^{L281Y} mutant exhibited a 2.7-fold increase in activity, and the TfCa^{I69W} mutant showed a 1.8-fold increase. The iterative mutant TfCa$^{I69W/L281Y}$ demonstrated a 3.5-fold increase in activity against MHET (Fig. S13). To assess whether TfCa$^{I69W/L281Y}$ would promote the degradation of PET by the multi-enzyme complex, it replaced wild-type TfCa to form a new whole-cell biocatalytic system. After a 24 h period of PET film degradation, TfCa$^{I69W/L281Y}$ demonstrated enhanced enzymatic cascade efficiency in PET film breakdown. The product release from the whole-cell biocatalytic system engineered with TfCa$^{I69W/L281Y}$ reached 0.66 ± 0.12 mM, representing a 2.5-fold increase compared to the wild-type TfCa assembly (Fig. 5A).

To comprehend the catalytic behavior of TfCa$^{I69W/L281Y}$, the structure of TfCa$^{I69W/L281Y}$ was predicted by FoldX and subsequently optimized by molecular dynamics simulation. In the wild-type TfCa, the hydrophobicity of the L281 keeps the hydrophilic Q263 further away, forming a 2.1-Å hydrogen bond between Q263 and Y320, resulting in a relatively small active pocket with a cross-section of approximately 6.5 Å in both length and width (Fig. 5B and C). Conversely, in the L281Y mutant, the hydrophilic Y induces a shift in the orientation of the side chain of Q263 to form a new hydrogen bond with L281Y at a distance of 2.0 Å, thereby resulting in a larger active pocket with cross-section measuring 11.6 Å in length and 6.7 Å in width (Fig. 5B and D). Such a result was further confirmed by the volume results of the substrate binding pocket of TfCa and TfCa$^{I69W/L281Y}$ using the POCASA 1.1 server. The volume of the substrate binding pocket of TfCa$^{I69W/L281Y}$ was 2347 Å^3, while that of TfCa was only 600 Å^3 (Fig. 5C and D). Moreover, root-mean-square fluctuations (RMSF) results revealed an enhanced oscillatory nature of the tryptophan residue at position 69, facilitating hydrophobic interactions with the substrate MHET (Fig. S14 and Table S2), suggesting that the W69 wobbliness of TfCa$^{I69W/L281Y}$ might enhance substrate binding, similar to the fact that W185 in *Is*PETase promoted PET binding [57]. In conclusion, the L281Y mutation altered the orientation of Q263, facilitating easier entry of MHET into the active center, while I69W increased flexibility for enhanced hydrophobic binding to MHET.

4. Conclusions

In this study, a multi-enzyme cascade system was successfully constructed. The corresponding PT-ECs of the three PETases exhibited excellent PET degradation efficiency, and even PT-EC^{EHA} showed a 16.5-fold increase in product release compared with PETase^{EHA} alone. Moreover, PT-EC^{ZPE} yielded 61.63 ± 0.19 mM of product for degradation of a gram-scale PET powder at 40 °C for 10 days, with a corresponding weight loss of 1.47 ± 0.02 g. Therefore, the results of this study further confirmed the feasibility of the multi-enzyme cascade system to efficiently degrade PET. Furthermore, PT-ECs were displayed on the surface of *E. coli*, and the displayed PT-ECs exhibited not only the high efficiency in the degradation of all tested PET types, but also the

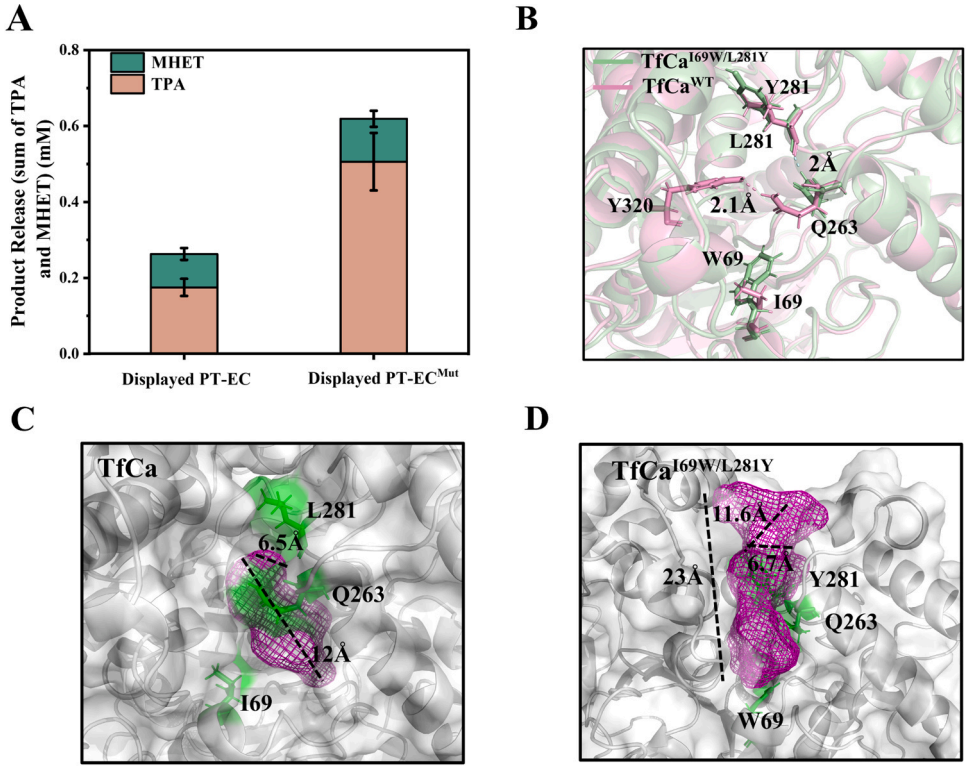

Fig. 5. Functional and structural analysis of TfCa$^{I69W/L281Y}$. (A) Evaluation of degradation of PET film by surface-displayed PT-EC assembled with TfCa$^{I69W/L281Y}$. (B) Structural comparison of activity pockets between TfCa$^{I69W/L281Y}$ and TfCa. Residues from different domains are indicated by red bars (TfCa) and green bars (TfCa$^{I69W/L281Y}$). The active cavity volumes of TfCa (C) and TfCa$^{I69W/L281Y}$ (D) were analyzed using the online server POCASA 1.1. The active cavity volume of TfCa is 600 Å^3 and the active cavity volume of TfCa$^{I69W/L281Y}$ is 2347 Å^3. The cross-section of the TfCa$^{I69W/L281Y}$ active pocket measures 11.6 Å in length and 6.7 Å in width, while that of TfCa is approximately 6.5 Å in both dimensions.

enhanced tolerance against organic solvent. The $TfCa^{I69W/L281Y}$ mutant, evolved through molecular docking-based virtual screening, further facilitated MHET conversion, thereby enhancing PET degradation by surface-displayed PT-ECs. Thus, in addition to evolved efficient enzymes and substrate binding motif, the multi-enzyme cascade system represents another promising strategy to facilitate PET biodegradation at near-ambient temperatures.

Environmental implication

The accumulation of polyethylene terephthalate (PET) in the environment poses a major ecological threat due to its resistance to degradation. Employing biodegradation as a sustainable and eco-friendly solution for PET has become imperative. In this study, a multi-enzyme complex (PT-EC) with a remarkable PET biodegradation capability under near-ambient conditions was constructed. Notably, the PT-EC self-assembled whole-cell biocatalytic system exhibited a substantial 20-fold enhancement in PET degradation efficiency compared to the exclusive surface display of $PETase^{EHA}$. These findings substantiate a multi-enzyme self-assembly system as a promising strategy for PET biodegradation.

CRediT authorship contribution statement

Qiuyue Si: Validation. **Linling Zhong:** Validation. **Yan Pan:** Validation. **Xianghong Liu:** Validation. **Qifa Jiang:** Validation. **Lizhu Aer:** Writing – original draft, Methodology, Investigation, Formal analysis, Data curation, Conceptualization. **Juan Feng:** Validation. **Tang Lixia:** Writing – review & editing, Supervision, Conceptualization. **Hongjuan Zeng:** Validation.

Declaration of Competing Interest

The authors declare that they have no known competing financial interests or personal relationships that could have appeared to influence the work reported in this paper.

Data availability

Data will be made available on request.

Acknowledgements

This work was supported by Medico-Engineering Cooperation Funds from the University of Electronic Science and Technology of China (ZYGX2021YGLH202).

Appendix A. Supporting information

Supplementary data associated with this article can be found in the online version at doi:10.1016/j.jhazmat.2024.134887.

References

[1] Kim, N.K., Lee, S.H., Park, H.D., 2022. Current biotechnologies on depolymerization of polyethylene terephthalate (PET) and repolymerization of reclaimed monomers from PET for bio-upcycling: a critical review. Bioresour Technol 363, 127931. https://doi.org/10.1016/j.biortech.2022.127931.

[2] Zhu, B., Ye, Q., Seo, Y., Wei, N., 2022. Enzymatic degradation of polyethylene terephthalate plastics by bacterial curli display PETase. Environ Sci Tech Let 9, 650–657. https://doi.org/10.1021/acs.estlett.2c00332.

[3] MacLeod, M., Arp, H.P.H., Tekman, M.B., Jahnke, A., 2021. The global threat from plastic pollution. Science 373, 61–65. https://doi.org/10.1126/science.abg5433.

[4] Chu, M., Liu, Y., Lou, X., Zhang, Q., Chen, J., 2022. Rational design of chemical catalysis for plastic recycling. ACS Catal 12, 4659–4679. https://doi.org/10.1021/acscatal.2c01286.

[5] Tournier, V., Duquesne, S., Guillamot, F., Cramail, H., Andre, I., Taton, D., Marty, A., 2023. Enzymes' power for plastics degradation. Chem Rev 123, 5612–5701. https://doi.org/10.1021/acs.chemrev.2c00644.

[6] Taniguchi, I., Yoshida, S., Hiraga, K., Miyamoto, K., Kimura, Y., Oda, K., 2019. Biodegradation of PET: current status and application aspects. ACS Catal 9, 4089–4105. https://doi.org/10.1021/acscatal.8b05171.

[7] Müller, R.J., Schrader, H., Profe, J., Dresler, K., Deckwer, W.D., 2005. Enzymatic degradation of poly(ethylene terephthalate): rapid hydrolyse using a hydrolase from *T. fusca*. Macromol Rapid Commun 26, 1400–1405. https://doi.org/10.1002/marc.200500410.

[8] Lee, S., Lee, Y.R., Kim, S.J., Lee, J.S., Min, K., 2023. Recent advances and challenges in the biotechnological upcycling of plastic wastes for constructing a circular bioeconomy. Chem Eng J 454, 140470. https://doi.org/10.1016/j.cej.2022.140470.

[9] Yoshida, S., Hiraga, K., Takehana, T., Taniguchi, I., Yamaji, H., Maeda, Y., Toyohara, K., Miyamoto, K., Kimura, Y., Oda, K., 2016. A bacterium that degrades and assimilates poly(ethylene terephthalate). Science 351, 1196–1199. https://doi.org/10.1126/science.aad6359.

[10] Liu, F., Wang, T., Yang, W., Zhang, Y., Gong, Y., Fan, X., Wang, G., Lu, Z., Wang, J., 2023. Current advances in the structural biology and molecular engineering of PETase. Front Bioeng Biotechnol 11, 1263996. https://doi.org/10.3389/fbioe.2023.1263996.

[11] Yin, Q., You, S., Zhang, J., Qi, W., Su, R., 2022. Enhancement of the polyethylene terephthalate and mono-(2-hydroxyethyl) terephthalate degradation activity of *Ideonella sakaiensis* PETase by an electrostatic interaction-based strategy. Bioresour Technol 364, 128026. https://doi.org/10.1016/j.biortech.2022.128026.

[12] Chen, X.Q., Guo, Z.Y., Wang, L., Yan, Z.F., Jin, C.X., Huang, Q.S., Kong, D.M., Rao, D.M., Wu, J., 2022. Directional-path modification strategy enhances PET hydrolase catalysis of plastic degradation. J Hazard Mater 433, 128816. https://doi.org/10.1016/j.jhazmat.2022.128816.

[13] Cui, Y., Chen, Y., Liu, X., Dong, S., Tian, Ye, Qiao, Y., Mitra, R., Han, J., Li, C., Han, X., Liu, W., Chen, Q., Wei, W., Wang, X., Du, W., Tang, S., Xiang, H., Liu, H., Liang, Y., Houk, K.N., Wu, B., 2021. Computational redesign of a PETase for plastic biodegradation under ambient condition by the GRAPE strategy. ACS Catal 11, 1340–1350. https://doi.org/10.1021/acscatal.0c05126.

[14] Lu, H., Diaz, D.J., Czarnecki, N.J., Zhu, C., Kim, W., Shroff, R., Acosta, D.J., Alexander, B.R., Cole, H.O., Zhang, Y., Lynd, N.A., Ellington, A.D., Alper, H.S., 2022. Machine learning-aided engineering of hydrolases for PET depolymerization. Nature 604, 662–667. https://doi.org/10.1038/s41586-022-04599-z.

[15] Shi, L., Liu, P., Tan, Z., Zhao, W., Gao, J., Gu, Q., Ma, H., Liu, H., Zhu, L., 2023. Complete depolymerization of PET wastes by an evolved PET hydrolase from directed evolution. Angew Chem Int Ed 62, e202218390. https://doi.org/10.1002/anie.202218390.

[16] Bell, E.L., Smithson, R., Kilbride, S., Foster, J., Hardy, F.J., Ramachandran, S., Tedstone, A.A., Haigh, S.J., Garforth, A.A., Day, P.J.R., Levy, C., Shaver, M.P., Green, A.P., 2022. Directed evolution of an efficient and thermostable PET depolymerase. Nat Catal 5, 673–681. https://doi.org/10.1038/s41929-022-00821-3.

[17] Son, H.F., Cho, I.J., Joo, S., Seo, H., Sagong, H.Y., Choi, S.Y., Lee, S.Y., Kim, K.J., 2019. Rational protein engineering of thermo-stable PETase from *Ideonella sakaiensis* for highly efficient PET degradation. ACS Catal 9, 3519–3526. https://doi.org/10.1021/acscatal.9b00568.

[18] Lee, S.H., Seo, H., Hong, H., Park, J., Ki, D., Kim, M., Kim, H.J., Kim, K.J., 2023. Three-directional engineering of *Is*PETase with enhanced protein yield, activity, and durability. J Hazard Mater 459, 132297. https://doi.org/10.1016/j.jhazmat.2023.132297.

[19] Erickson, E., Shakespeare, T.J., Bratti, F., Buss, B.L., Graham, R., Hawkins, M.A., Konig, G., Michener, W.E., Miscall, J., Ramirez, K.J., Rorrer, N.A., Zahn, M., Pickford, A.R., McGeehan, J.E., Beckham, G.T., 2022. Comparative performance of PETase as a function of reaction conditions, substrate properties, and product accumulation. ChemSusChem 15, e202101932. https://doi.org/10.1002/cssc.202101932.

[20] Giannakopoulou, A., Gkantzou, E., Polydera, A., Stamatis, H., 2020. Multienzymatic nanoassemblies: recent progress and applications. Trends Biotechnol 38, 202–216. https://doi.org/10.1016/j.tibtech.2019.07.010.

[21] Aer, L., Qin, H., Wo, P., Feng, J., Tang, L., 2024. Signal peptide independent secretion of bifunctional dual-hydrolase to enhance the bio-depolymerization of polyethylene terephthalate. Bioresour Technol 391, 129884. https://doi.org/10.1016/j.biortech.2023.129884.

[22] Knott, B.C., Erickson, E., Allen, M.D., Gado, J.E., Graham, R., Kearns, F.L., Pardo, I., Topuzlu, E., Anderson, J.J., Austin, H.P., Dominick, G., Johnson, C.W., Rorrer, N.A., Szostkiewicz, C.J., Copie, V., Payne, C.M., Woodcock, H.L., Donohoe, B.S., Beckham, G.T., McGeehan, J.E., 2020. Characterization and engineering of a two-enzyme system for plastics depolymerization. PNAS 117, 25476–25485. https://doi.org/10.1073/pnas.2006753117.

[23] Chen, K., Dong, X., Sun, Y., 2022. Sequentially co-immobilized PET and MHET hydrolases via Spy chemistry in calcium phosphate nanocrystals present high-performance PET degradation. J Hazard Mater 438, 129517. https://doi.org/10.1016/j.jhazmat.2022.129517.

[24] Zhang, J., Wang, H., Luo, Z., Yang, Z., Zhang, Z., Wang, P., Li, M., Zhang, Y., Feng, Y., Lu, D., Zhu, Y., 2023. Computational design of highly efficient thermostable MHET hydrolases and dual enzyme system for PET recycling. Commun Biol 6. https://doi.org/10.1038/s42003-023-05523-5.

[25] Sagong, H.Y., Seo, H., Kim, T., Son, H.F., Joo, S., Lee, S.H., Kim, S., Woo, J.S., Hwang, S.Y., Kim, K.J., 2020. Decomposition of the PET film by MHETase using exo-PETase function. ACS Catal 10, 4805–4812. https://doi.org/10.1021/acscatal.9b05604.

[26] Haugwitz, G., Han, X., Pfaff, L., Li, Q., Wei, H., Gao, J., Methling, K., Ao, Y., Brack, Y., Mican, J., Feiler, C.G., Weiss, M.S., Bednar, D., Palm, G.J., Lalk, M.,

Lammers, M., Damborsky, J., Weber, G., Liu, W., Bornscheuer, U.T., Wei, R., 2022. Structural Insights into (tere)phthalate-ester hydrolysis by a carboxylesterase and its role in promoting PET depolymerization. ACS Catal 12, 15259–15270. https://doi.org/10.1021/acscatal.2c03772.

[27] Shah, A.A., Hasan, F., Hameed, A., Ahmed, S., 2008. Biological degradation of plastics: a comprehensive review. Biotechnol Adv 26, 246–265. https://doi.org/10.1016/j.biotechadv.2007.12.005.

[28] Puspitasari, N., Tsai, S.L., Lee, C.K., 2021. Class I hydrophobins pretreatment stimulates PETase for monomers recycling of waste PETs. Int J Biol Macromol 176, 157–164. https://doi.org/10.1016/j.ijbiomac.2021.02.026.

[29] Ribitsch, D., Yebra, A.O., Zitzenbacher, S., Wu, J., Nowitsch, S., Steinkellner, G., Greimel, K., Doliska, A., Oberdorfer, G., Gruber, C.C., Gruber, K., Schwab, H., Stana-Kleinschek, K., Acero, E.H., Guebitz, G.M., 2013. Fusion of binding domains to thermobifida cellulosilytica cutinase to tune sorption characteristics and enhancing PET hydrolysis. Biomacromolecules 14, 1769–1776. https://doi.org/10.1021/bm400140u.

[30] Artzi, L., Bayer, E.A., Morais, S., 2017. Cellulosomes: bacterial nanomachines for dismantling plant polysaccharides. Nat Rev Microbiol 15, 83–95. https://doi.org/10.1038/nrmicro.2016.164.

[31] Gamerith, C., Herrero Acero, E., Pellis, A., Ortner, A., Vielnascher, R., Luschnig, D., Zartl, B., Haernvall, K., Zitzenbacher, S., Strohmeier, G., Hoff, O., Steinkellner, G., Gruber, K., Ribitsch, D., Guebitz, G.M., 2016. Improving enzymatic polyurethane hydrolysis by tuning enzyme sorption. Polym Degrad Stabil 132, 69–77. https://doi.org/10.1016/j.polymdegradstab.2016.02.025.

[32] Chen, Z., Duan, R., Xiao, Y., Wei, Y., Zhang, H., Sun, X., Wang, S., Cheng, Y., Wang, X., Tong, S., Yao, Y., Zhu, C., Yang, H., Wang, Y., Wang, Z., 2022. Biodegradation of highly crystallized poly(ethylene terephthalate) through cell surface codisplay of bacterial PETase and hydrophobin. Nat Commun 13, 7138. https://doi.org/10.1038/s41467-022-34908-z.

[33] Aer, L., Jiang, Q., Gul, I., Qi, Z., Feng, J., Tang, L., 2022. Overexpression and kinetic analysis of *Ideonella sakaiensis* PETase for polyethylene terephthalate (PET) degradation. Environ Res 212, 113472. https://doi.org/10.1016/j.envres.2022.113472.

[34] Anandharaj, M., Lin, Y.J., Rani, R.P., Nadendla, E.K., Ho, M.C., Huang, C.C., Cheng, J.F., Chang, J.J., Li, W.H., 2020. Constructing a yeast to express the largest cellulosome complex on the cell surface. PNAS 117, 2385–2394. https://doi.org/10.1073/pnas.1916529117.

[35] Hwang, E.T., Lee, S., 2019. Multienzymatic cascade reactions via enzyme complex by immobilization. ACS Catal 9, 4402–4425. https://doi.org/10.1021/acscatal.8b04921.

[36] Liu, Z., Cao, S., Liu, M., Kang, W., Xia, J., 2019. Self-assembled multienzyme nanostructures on synthetic protein scaffolds. ACS Nano 13, 11343–11352. https://doi.org/10.1021/acsnano.9b04554.

[37] Schymkowitz, J., Borg, J., Stricher, F., Nys, R., Rousseau, F., Serrano, L., 2005. The FoldX web server: an online force field. Nucleic Acids Res 33, W382–W388. https://doi.org/10.1093/nar/gki387.

[38] Eberhardt, J., Santos-Martins, D., Tillack, A.F., Forli, S., 2021. Autodock vina 1.2.0: new docking methods, expanded force field, and python bindings. J Chem Inf Model 61, 3891–3898. https://doi.org/10.1021/acs.jcim.1c00203.

[39] Abraham, M.J., Murtola, T., Schulz, R., Páll, S., Smith, J.C., Hess, B., Lindahl, E., 2015. GROMACS: high performance molecular simulations through multi-level parallelism from laptops to supercomputers. SoftwareX 1, 19–25. https://doi.org/10.1016/j.softx.2015.06.001.

[40] Van Der Spoel, D., Lindahl, E., Hess, B., Groenhof, G., Mark, A.E., Berendsen, H.J. C., 2005. GROMACS: fast, flexible, and free. J Comput Chem 26, 1701–1718. https://doi.org/10.1002/jcc.20291.

[41] Chen, C.C., Han, X., Ko, T.P., Liu, W., Guo, R.T., 2018. Structural studies reveal the molecular mechanism of PETase. FEBS J 285, 3717–3723. https://doi.org/10.1111/febs.14612.

[42] Austin, H.P., Allen, M.D., Donohoe, B.S., Rorrer, N.A., Kearns, F.L., Silveira, R.L., Pollard, B.C., Dominick, G., Duman, R., El Omari, K., Mykhaylyk, V., Wagner, A., Michener, W.E., Amore, A., Skaf, M.S., Crowley, M.F., Thorne, A.W., Johnson, C. W., Woodcock, H.L., McGeehan, J.E., Beckham, G.T., 2018. Characterization and engineering of a plastic-degrading aromatic polyesterase. PNAS 115, E4350–E4357. https://doi.org/10.1073/pnas.1718804115.

[43] Graham, R., Erickson, E., Brizendine, R.K., Salvachúa, D., Michener, W.E., Li, Y., Tan, Z., Beckham, G.T., McGeehan, J.E., Pickford, A.R., 2022. The role of binding modules in enzymatic poly(ethylene terephthalate) hydrolysis at high-solids loadings. Chem Catal 2, 2644–2657. https://doi.org/10.1016/j.checat.2022.07.018.

[44] Zhang, Y., Wang, L., Chen, J., Wu, J., 2013. Enhanced activity toward PET by site-directed mutagenesis of *Thermobifida fusca* cutinase-CBM fusion protein. Carbohydr Polym 97, 124–129. https://doi.org/10.1016/j.carbpol.2013.04.042.

[45] Weber, J., Petrović, D., Strodel, B., Smits, S.H.J., Kolkenbrock, S., Leggewie, C., Jaeger, K.E., 2019. Interaction of carbohydrate-binding modules with poly (ethylene terephthalate). Appl Microbiol Biotechnol 103, 4801–4812. https://doi.org/10.1007/s00253-019-09760-9.

[46] Chen, Y., Zhang, S., Zhai, Z., Zhang, S., Ma, J., Liang, X., Li, Q., 2023. Construction of fusion protein with carbohydrate-binding module and leaf-branch compost cutinase to enhance the degradation efficiency of polyethylene terephthalate. Int J Mol Sci 24, 2780. https://doi.org/10.3390/ijms24032780.

[47] Zhou, J., Harindintwali, J.D., Yang, W., Han, M., Deng, B., Luan, H., Zhang, W., Liu, X., Yu, X., 2021. Engineering of a chitosanase fused to a carbohydrate-binding module for continuous production of desirable chitooligosaccharides. Carbohydr Polym 273, 118609. https://doi.org/10.1016/j.carbpol.2021.118609.

[48] Li, H., Lu, Z., Hao, M.S., Kvammen, A., Inman, A.R., Srivastava, V., Bulone, V., McKee, L.S., 2023. Family 92 carbohydrate-binding modules specific for β-1,6-glucans increase the thermostability of a bacterial chitinase. Biochimie 212, 153–160. https://doi.org/10.1016/j.biochi.2023.04.019.

[49] Zeng, Y., Xu, J.Y., Fu, X.P., Tan, M., Liu, F., Zheng, H.C., Song, H., 2019. Effects of different carbohydrate-binding modules on the enzymatic properties of pullulanase. Int J Biol Macromol 137, 973–981. https://doi.org/10.1016/j.ijbiomac.2019.07.054.

[50] Wösten, H.A., Schuren, F.H., JG, W., 1994. Interfacial self-assembly of a hydrophobin into an amphipathic protein membrane mediates fungal attachment to hydrophobic surfaces. EMBO J 13, 5848–5854. https://doi.org/10.1002/j.1460-2075.1994.tb06929.x.

[51] Schrewe, M., Julsing, M.K., Bühler, B., Schmid, A., 2013. Whole-cell biocatalysis for selective and productive C–O functional group introduction and modification. Chem Soc Rev 42, 6346–6377. https://doi.org/10.1039/c3cs60011d.

[52] Han, W., Zhang, J., Chen, Q., Xie, Y., Zhang, M., Qu, J., Tan, Y., Diao, Y., Wang, Y., Zhang, Y., 2024. Biodegradation of poly(ethylene terephthalate) through PETase surface-display: from function to structure. J Hazard Mater 461, 132632. https://doi.org/10.1016/j.jhazmat.2023.132632.

[53] Heinisch, T., Schwizer, F., Garabedian, B., Csibra, E., Jeschek, M., Vallapurackal, J., Pinheiro, V.B., Marlière, P., Panke, S., Ward, T.R., 2018. *E. coli* surface display of streptavidin for directed evolution of an allylic deallylase. Chem Sci 9, 5383–5388. https://doi.org/10.1039/c8sc00484f.

[54] Khairil Anuar, I.N.A., Banerjee, A., Keeble, A.H., Carella, A., Nikov, G.I., Howarth, M., 2019. Spy&go purification of spytag-proteins using pseudo-spycatcher to access an oligomerization toolbox. Nat Commun 10, 1734. https://doi.org/10.1038/s41467-019-09678-w.

[55] Avilan, L., Lichtenstein, B.R., König, G., Zahn, M., Allen, M.D., Oliveira, L., Clark, M., Bemmer, V., Graham, R., Austin, H.P., Dominick, G., Johnson, C.W., Beckham, G.T., McGeehan, J.E., Pickford, A.R., 2023. Concentration-dependent inhibition of mesophilic PETases on poly(ethylene terephthalate) can be eliminated by enzyme engineering. Chemsuschem 16, e202202277. https://doi.org/10.1002/cssc.202202277.

[56] Chen, Y.G., Zhang, Y., Zhang, Z.Z., 2021. Occurrence, effects, and biodegradation of plastic additives in sludge anaerobic digestion: a review. Environ Pollut 287, 117568. https://doi.org/10.1016/j.envpol.2021.117568.

[57] Han, X., Liu, W., Huang, J.W., Ma, J., Zheng, Y., Ko, T.P., Xu, L., Cheng, Y.S., Chen, C.C., Guo, R.T., 2017. Structural insight into catalytic mechanism of PET hydrolase. Nat Commun 8, 2106. https://doi.org/10.1038/s41467-017-02255-z.